Paleotsunami deposits along the coast of Egypt correlate with historical earthquake records of eastern Mediterranean

A. Salama, (1, 2, *), M. Meghraoui (1**), M. El Gabry (2, *),
S. Maouche (3, *), H. M. Hussein (2, *), and I. Korrat (4)

[1.] EOST-IPGS - CNRS - UMR 7516, Strasbourg, France
[2.] NRIAG, 11421 Helwan, Egypt
[3.] CRAAG, Bouzareah, Algeria
[4.] Mansoura University, Mansoura, Egypt

* Also at *North Africa Group for Earthquake and Tsunami Studies (NAGET), Ne t40/OEA ICTP, Italy*

***Corresponding author*

Submitted to Natural Hazards and *and Earth System Sciences* (*NHESS*)
Revised version July 2018

Abstract.

We study the sedimentary record of past tsunamis along the coastal area west of Alexandria (NW Egypt) taking into account the occurrence of major historical earthquakes in the eastern Mediterranean. The two selected sites at Kefr Saber (~32-km west of Marsa-Matrouh city) and ~10 km northwest of El Alamein village are coastal lagoons protected by 2 to 20-m-high dunes parallel to the shoreline. Field data were collected by: 1) Coastal geomorphology along estuaries, wedge-protected and dune-protected lagoons; and 2) identification and spatial distribution of paleotsunamis deposits using five trenches (1.5-m-depth) at Kefr Saber and twelve cores (1 to 2.5-m-depth) at El Alamein. Detailed logging of sedimentary sections was conducted using X rays, grain size and sorting, total organic and inorganic matter, bulk mineralogy, magnetic susceptibility and radiocarbon dating to identify past tsunamis records. Generally of low energy, the stratigraphic succession made of coastal lagoon and alluvial deposits includes intercalated high-energy deposits made of mixed fine and coarse sand with broken shells, interpreted as catastrophic layers correlated with tsunami deposits. Radiocarbon dating of 46 samples consist in mixed old (> 13000 year BP) and young (< 5500 year BP), dated charcoal and shells in sedimentary units correlate with the 24 June 1870 (Mw 7.5), 8 August 1303 (Mw ~8) and 21 July 365 (Mw 8 – 8.5) large tsunamigenic earthquakes that caused inundation along the Alexandria and northern Egyptian shoreline. Our results point out the size and recurrence of past tsunamis and the potential for future tsunami hazard over the Egyptian coastline and the eastern Mediterranean regions.

Key words: paleotsunami, coring, trenching, coastal geomorphology, northern Egypt

1. Introduction:

Egypt has a well-documented historical catalogue of earthquakes and tsunamis recorded in ancient texts and manuscripts. Original documents and archives from past civilizations are considered the principal sources of macroseismic data for major historical earthquakes and tsunamis (Poirier and Taher, 1980; Maamoun et al., 1984; Ambraseys et al., 1994, 2009; Guidoboni et al., 1994, 2005; Soloviev et al. 2000, Tinti et al., 2001). The catalogue of Ambraseys et al., 2009 reports that coastal cities of northern Egypt have experienced repeated tsunami inundation with severe damage in the past. While historical earthquakes and tsunamis are well documented, it appears that there is a lack of holistic investigations for tsunami deposits along the Mediterranean coastlines. The geomorphology along the Mediterranean coastline of northern Egypt, with low-level topography (Hassouba, 1995), dunes and lagoons, constitutes an ideal natural environment for the geological record of past tsunamis.

The Eastern Mediterranean region has experienced major earthquakes (with Mw > 7.5), mainly along the Hellenic subduction zone, due to the convergence between the Eurasian and African plates (Fig. 1; Ambraseys et al., 1994, Taymaz et al., 2004). Major historical tsunamis in the eastern Mediterranean region which affected northern Egypt are triggered by large earthquakes (Papadopoulos et al., 2014). However, there is a possibility of landslide triggered tsunamis associated with local earthquakes (El-Sayed et al., 2004; Tinti et al., 2005). Yalciner et al. (2014) estimated from modelling that a landslide with a volume up to 500 km^3 may have caused a tsunami with a wave height ranging from 0.4 to 4 m offshore of the Nile Delta. Coastal landslides may generate giant tsunamis as the Storrega event that impacted Norway and the North Atlantic Ocean in ~6100 BC (Bondevik et al., 2012).

Tsunami research of the past 20 years has led to the discovery of coastal tsunami sedimentary records dating back to thousands of years. Among the early studies was that of

Atwater (1987) who found evidence of more than six soil layers buried below tsunami deposits over the past 7000 years along the Puget Sound coastline of Washington State. Costa et al., (2014), studied the sedimentological records and related microtexture and heavy mineral assemblage for three events in Portugal in AD 1755, Scotland in 8200 calendar year BP and in Indonesia associated with the 2004 Sumatra earthquake. Sawai (2001) and Nanayama et al. (2003) recognized major tsunamis due to extensive coastal inundation along the eastern coast of Hokkaido (northern Japan); the repeated sand sheet layers several kilometres inland evidenced a 500-year tsunami cycle in the period between 2000 and 7000 years BP. Following the 2004 Sumatra earthquake (Mw 9.1) and in addition to the coral reef uplift and subsidence (Meltzner et al; 2009), Malik et al. (2015) identified (in trenches) three historical tsunamis during the past 1000 years along the coast of South Andaman Island (India). Lario et al. (2011) document five tsunami events in the Gulf of Cadiz (Spain) generated by strong earthquakes in the last 7000 years, prior to 1755 AD Lisbon earthquake generated tsunami. In the Mediterranean, De Martini et al. (2012) identified two tsunami deposits during the first millennium BC and another one in 650-770 AD and estimated a 385 year average recurrence interval for strong tsunamis along the eastern coast of Sicily (Italy). Minoura et al. (2000) described tsunami deposits with volcanic ashes along the coast in Crete (Greece) that correlate with Thera (Santorini) eruption in late Minoan time (1600–1300 B.C.). Papadopoulos et al. (2012) documented three paleotsunami layers attributed to the 1303, 1481 and 1741 historically documented tsunamis in Dalaman (SW Turkey). Using granulometry, XRD, XRF and FT-IR, Tyuleneva et al. (2017) identified two sedimentary events offshore of Casearea (Israel) that may correlate with landslide tsunamis in AD 749 and 5700 BP (Chalcolithic cultural period).

In this paper, we investigate the high energy sedimentary deposits along the northern coast of Egypt and their correlation with the historical tsunami catalogue of the Eastern

Mediterranean. Using coastal geomorphology with trenching and coring, we examine the geological evidence of tsunami deposits using textural, geochemical analysis, magnetic susceptibility and radiocarbon dating to identify the tsunamis records. We have analysed 120 samples (25 grams each) from core tubes every 15 cm for the geochemical analysis including grain size, bulk mineralogy and totally organic and inorganic matter. The magnetic susceptibility was measured every 3 cm in cores. The Bayesian simulation (Oxcal 4.2; Bronk-Ramsey, 2009) is applied to the radiocarbon results and stratigraphic succession of coastal deposits in order to generate a precise paleochronology of tsunami events.

2. Major historical tsunamis of the Mediterranean coast of Egypt

The tsunami catalogue of Egypt cites the work of Ambraseys (2005) who report several large historical tsunamigenic earthquakes with severe damage in the eastern Mediterranean regions (Table 1). Among these events, the tsunamis of 21 July 365, 8 August 1303 and 24 June 1870 inundated the harbour of Alexandria city as well as the Mediterranean coast of Egypt.

Early in the morning of 21 July 365, an earthquake with estimated magnitude ~Mw 8-8.5 located offshore West of Crete, generated a major tsunami that affected the eastern Mediterranean coastal regions (Ambraseys et al., 1994). The Roman historian Ammianus Marcellinus (Guidoboni et al., 1994) reported sudden shaking with the occurrence of a “gigantic” wave moving toward the Mediterranean coastal areas. The tsunami wave caused great damage to the Alexandria harbour and city. The ships were inundated up to house roofs due to the effect of tsunami waves. As modelled by Hamouda (2009), the estimated wave height of this tsunami was greater than 8 m in Alexandria. The seismic source of this earthquake is located in western Crete, according to archaeological and historical damage distribution, combined with coastal uplift measurements and modelling (Fig. 1; Guidoboni et al., 1994; Stiros, 2001; Shaw et al., 2008 and Ambraseys, 2009).

On 8 August 1303 a major earthquake with magnitude ~Mw 8 located between Crete and Rhodes islands (Fig.1) generated a tsunami that greatly damaged the coastal cities of the eastern Mediterranean (Ambraseys, 2009, Papadopoulos et al. 2014). Abu-El Fida (1907) reported that the Alexandria city and the Nile Delta were flooded in 1329 and many houses were damaged in Cairo and northern Egypt. In Alexandria, part of the city walls collapsed, the famous lighthouse was destroyed and some ships were torn apart and carried inland by the tsunami waves (Abu-El Fida, 1907).

On 24 June 1870, a large earthquake affected many places of the eastern Mediterranean region and was felt in Alexandria at around 1800 h with no damage in the city but with slight damage in Cairo (Ambraseys, 2009). Along the Alexandria coastline and the Nile Delta, the sea waves flooded the docks of ports and inland fields (Coumbary, 1870). The epicentre location of this earthquake at eastern edge of Crete is inferred from damage in Heraklion and related shaking felt around the east Mediterranean (Fig. 1; Schmidt, J.F., 1879; Jusseret and Sintubin, 2017).

The AD 365 and AD 1303 events were classified as very large earthquakes (with Mw ≥ 8; Stiros et al., 2001; Shaw et al., 2008; Hamouda, 2006, 2009) that generated major tsunamis with basin-wide impacts, while the 1870 earthquake was of a lower magnitude (Mw ~7 – 7.5; Ben Menahem et al., 1991; Soloviev, 2000). Several studies of the 21 July 365 and 8 August 1303 historical earthquakes and associated tsunami waves report inundation in Alexandria and the coastlines of northern Egypt. Therefore there is the potential of tsunami records in the sedimentary deposits. There have been some debates on the 1870 event’s location, size and the possibility of tsunami waves, but several authors (Soloviev et al., 2000;

Ben Menahem et al., 1979; Salamon et al., 2007; Papadopoulos et al., 2010; and Maramai et al., 2014) support the tsunami generation by 1870 earthquake.

3. Coastal geomorphology and site selection for paleotsunami records

The northwest Mediterranean coast of Egypt forms the northern extremity of the Marmarica plateau which is a Miocene homoclinal limestone that extends west of Alexandria for about 500 km (Sayed, 2013), acting as a major catchment area feeding the drainage system (Fig. 1). The plateau runs from the Qattara Depression in the south to the piedmont plain in the north with variable elevation reaching a maximum of ~100 m at Marsa Matrouh escarpment. The geomorphological landform of the study area is characterized by a 60-m-high northern plateau that includes ridges, sand dunes, lagoons, and rocky plains within a 20-km-wide strip along the coastline (Fig. 1). The rocky Pleistocene limestone ridges include a veneer of carbonate sand that are mostly composed of oolitic grains (Frihy et al., 2010).

The beach-dune ridge is developed along the receding Quaternary shorelines and embayment of the Mediterranean Sea (Hassouba, 1995). Coastal dune-ridges protect inner lagoons from the sea and constitute outstanding landform features at several locations parallel to the shoreline (Figs 2). When the sand dunes are removed they leave rocky headland outcrops (Abbas et al., 2008). The 2 to 20-m-high coastal beach-dune ridges are mainly composed of oolitic and biogenic calcareous sand and separate the coastal lagoons and sabkhas (salt lake) from the sea. The lagoons with flat depressions separated from the sea by the coastal dunes (with different heights and sometimes with seawater outlets) are likely sites for the record of past tsunami deposits.

The accumulation of large boulders (Shah-Hosseini et al., 2016) near the selected sites is considered as a possible indication of past tsunami events. However, the boulders along the coastlines may either result from storms (Hall et al. 2006; Spiske et al. 2008) or tsunami waves (Goff et al. 2006; 2009; Morhange et al. 2006). The imbricated surface observed on large boulders near our investigation sites is directed towards the south. These boulders appear to be displaced by strong waves from the Mediterranean, and they are very similar to the tsunami boulders studied along the Algerian coastline (Maouche et al. 2009).

The discrimination between storm and tsunami deposits is a challenge in the Mediterranean region (Maouche et al., 2009; Marriner et al., 2017). However, in comparison with the high frequency of storm events and possible related deposits (Lionello et al., 2006), the tsunami stratigraphic record is less recurrent (according to Tinti et al., 2001; Morton et al., 2007) and often presents a specific sedimentary signature of mixed deposits such as: 1) the basal contact of tsunami layer is extremely sharp with loadcast sedimentary structures where layers contain organic rich mud and vegetation (Matsumoto et al., 2008; Switzer and Jones 2008); 2) the presence of rip up clasts that suggest considerable erosion of lagoon and soil deposits usually associated with tsunami deposits (Szczuciński et al 2006); 3) tsunami deposits show general tendency of thinning landward as shown by the 2011 Tohoku-oki earthquake tsunami in Hasunuma and by the 2004 Sumatra earthquake tsunami in Thailand (Matsumoto et al., 2016); 4) concentration of heavy minerals assemblages decreases upward within the tsunami layer (Costa et al., 2014); 5) the low peak value of magnetic susceptibility linked to the amount of sand originated from the littoral dunes and reworked mixed sediments from tsunami waves (Font et al., 2010); 6) the large number of mixed broken bivalve shells and gastropods occupy vertical and horizontal stratigraphic positions due to high wave current (Donato et al., 2008); 7) the tsunami deposits tendency of being poorly sorted, with bimodal grain particle size as compared with the storm grain size which tends to be unimodal (Paris et al., 2007); and 8) the saltwater inundation during a tsunami event indicated by chemical analysis which is used as evidence of paleotsunami waves (Chagué et al., 2011).

The local geomorphological and topographic settings contribute to the site selection for paleotsunami investigations. Our site selection for trenching and coring took into account the accessibility to dry lagoons (during summer season) in areas with no urbanization or artificially reworked soil. Suitable sites for trenching and coring are located in areas protected from the sea by the rather low (~2-m-high) sand dune topography that allows tsunami waves and related material to deposit into the lagoon. Two sites (~200 km part) within seasonally dry lagoons have met the selection criteria for paleotsunami investigation (Figs. 1 and 2): 1) Kefr Saber located ~32-km west of Marsa-Matrouh city; and 2) El Alamein site, ~10 km northwest of El Alamein city and ~150 km west of Alexandria. Five trenches were dug at Kefr Saber (Fig 2a), and 12 cores were performed at the El Alamein site (Fig 2b).

4. Methods for paleotsunami investigations

The trench size is typically ~2 x 1-m and ~1.5-m-depth depending on the depth of the water table. All trench walls exposed fine-grained sedimentary layers that were logged in detail. The conventional cores were distributed in the lagoon area from the depression to the outlet of sea water in order to observe the thickness variations of high energy sedimentary layers. The maximum core depth reached was ~2.6 m.

The core tubes were split in half lengthwise, photographed using both normal and ultra-violet lightning accompanied by detailed description of textures and sedimentary structures. X-ray scanning was performed immediately after core opening and all cores were sent to the laboratory of the National Institute of Geophysics and Astronomy (NRIAG, Cairo) for sampling and further analysis. The magnetic susceptibility measurements were conducted along cores and samples were collected for radiocarbon dating, physical, chemical and organic matter analyses.

The magnetic susceptibility for the cores was measured every 3 cm at the NRIAG Rock Magnetism laboratory then corrected against air by using Bartington compatible software. A total of 120 samples (25 grams each) were collected from cores every 15 cm for geochemical analysis and then for: a) grain size analysis which includes separating the weighed samples through a series of sieves from 0.75 to 1000 microns. Statistics of the grain-size distribution were calculated using Folk and Ward (1957) to obtain mean grain-size and sorting of the sediments along the cores (see supplementary material, Tables S13 – S24 and Figs.S16-S27); b) bulk mineralogy (X-ray diffraction using a Philips PW 1730 measurement). The intensity of the most intense diffraction peak of each mineral (see supplementary material, Tables S1-12 and Figs.S4-S15) was measured and the identification of crystalline substance and crystalline phases in a specimen is achieved by comparing the specimen diffraction spectrum with spectra of known crystalline substances (according to the International Centre for Diffraction Data - ICDD); and c) the total organic and inorganic measurements were carried out at the laboratory of Central Metallurgical Research & Development Institute (CMRDI at Eltebbin, Egypt).

Three laboratories (Poznan laboratory in Poland, CIRAM in France and Beta Analytical laboratory in USA) conducted the radiocarbon AMS dating of samples in order to ensure consistency of results (see Tables 2 a and b). The collected samples are made of charcoal, bones, gastropods, shells and organic matter. The radiocarbon dating results of samples are subsequently corrected using a recent calibration curve (Reimer et al., 2013) and the Oxcal software (Bronk-Ramsay, 2009) for the probability density function with 2σ uncertainty for each dated sample. In addition, from a succession of calibrated dates, a Bayesian analysis provides the simulated age in a probability density function of a catastrophic event. The simulated age allows the correlation between the high energy sedimentary deposits, the related isotopic chronology and the historical tsunami events in catalogues.

5. Description of sedimentary layers in trenches and cores with C14 dating results

The selected sites revealed a succession of sedimentary units typical of lagoon deposits with fine strata made of a mix of fine gravel, sand, silt and clay (Salama, 2017). At both Kefr Saber and El Alamein sites, trenches and cores present comparable soft sediment content and stratigraphy. The variation of sediments contained in the different cores is due to the distance from the shore and to the core location within the lagoons with regard to dunes heights. A detailed description of the trenches and cores at both Kefr Saber and El Alamein sites is presented here below:

5. 1. Kefr Saber site: Trenches P1, P2, P3 and P4 are 40 to 154 meters distance from the shoreline and have quite similar sedimentary succession with fine-grained mostly alluvial deposits made of sandy-silty layers with mixed coarse and white fine sand that contains broken shells of marine origin (Fig. 3 and trench logs in supplemental material S1). A conspicuous layer of white mixed sand, gravel and broken shells with variable 2 to 15 cm thicknesses is found 25 – 55 cm below surface in P1, P2, P3; its thickness decreases landward to 1 cm in P4 (see supplemental material S1 a, b, c, d, e). Trench P5, which is close to the dunes and shoreline, shows a succession of coarse and fine sand and 30 to 40 cm thick mixed with pebbles which, as observed in other trenches, are fining inland.

The mixed radiocarbon dating of samples in trenches is an issue at Kefr Saber. Two charcoal samples collected in Trench P1 at 35 cm and 53 cm depth yield modern age (younger than 1650 AD) and 39000-38250 BC, respectively. In Trench P3, two other charcoal samples collected at 73 cm and 100 cm below the surface and both below the high energy sedimentary layer labelled 1 (Fig. S1-b) indicate 50 - 70 AD and 5300-5070 BC, respectively (see Table 2a). In Trench P4, four charcoal samples collected at 15 cm, 25 cm, 40 cm and 61 cm depth reveal modern ages (younger than 1650 AD). A fifth charcoal sample recovered at 60 cm below surface provides 17200 - 15900 BC. In Trench P5, four charcoal samples are collected, with the uppermost sample located at 12 cm depth is dated at 360-50 BC, the second sample at 17 cm depth show 30 - 180 AD, the third, and fourth charcoal samples found at 33 cm and 37 cm depth are dated at 350 - 1050 BC and 2400-4000BC, respectively. The mixing of old (older than 7000 years BP) and relatively young ages (younger than 2000 years BP) points to reworking of former deposits and redeposit into the lagoon.

Results: Although the sedimentary deposits in trenches at Kefr Saber indicate mixed and reworked sedimentation, the well identified coarse and fine white sand layer with broken shells of marine origin located between 25 - 55 cm below surface in trenches P1, P2, P3, P4 suggests a single homogeneous sedimentary unit of relatively young age deposited in the lagoon. Considering the deposits of neighboring trenches at Kefr Saber, and their relative sedimentary chronology of units deposited in the same lagoon, and taking into the possible reworked deposits that may include older ages, we selected the radiocarbon dates younger than 2000 year BP that bracket the white sandy layer unit (i.e., samples TSU P5 S4 and S5, TSU P3 S1 and S3 that predate the unit, and sample TSU P3 S2 that postdates the unit).

5. 2. El Alamein site*:* The 12 cores extend between 1 m and 2.6 m depth. Except, for cores 1 and 9, which are shown in Figures 5 a and b, the detailed stratigraphic logs and related measurements are presented in supplemental material S2. In a previous reconnaissance field investigation, a coarse and fine white sand layer was identified at ~ 30 cm below surface in a test pit. Two charcoal samples El Al sa1 and El Al sa2 collected at 25 cm and 56 cm depth gave ages of 1680-1908 AD and 1661-1931 AD respectively. The description of cores is as follows:

Core 1: This core is located ~166 m from the shoreline (Fig. 2 b), east of the study area behind the sand dunes and near the outlet of the seawater. The core depth reached ~2.14 m and the stratigraphic section includes four high energy sedimentary layers recognized as follows (Fig. 5 a section 1 and its continuation at depth in Fig. S2-1):

The first layer (~34.5 thick) located at ~12.5 cm depth is made of brown clay fine grained sediments, poorly sorted, with low peak in magnetic susceptibility, rich in organic matter, and X-ray image reflects clear lamination. The second layer (~5 cm thick) is located at ~70 cm depth and characterized by highly broken shells fragments with the very poor sorting of sediments. The third layer (~22 cm thick) at ~75 cm depth is made of pale yellow sand with poor sorting of sediments, and a high peak in magnetic susceptibility. The chemical analysis shows the presence of gypsum and minor goethite, and X-ray scanning shows some turbiditic current structures with rip clasts, crossbedding and laminations. A fourth high energy sedimentary layer is identified at 158 cm depth (see Fig. S2-1). It is characterized by pale brown silty clay, with broken shell fragments and extremely poor sorting, and with a high peak of magnetic susceptibility at the base of the layer.

Two samples were collected for radiocarbon dating from core 1. The first and uppermost sample is a charcoal fragment 40 cm below the surface located within a mixed sedimentary unit characterized by poor sorting, highly broken shell fragments and the low peak value of magnetic susceptibility.

Core 2: As shown in (Fig.S2-2), the core is ~90 cm deep and located ~264 m from the shoreline (Fig. 2 b). Two high energy sedimentary layers are identified. The first layer is a ~12 cm thick brown clay sediments at ~13 cm depth mixed with gravel and sand. The layer is rich in organic matter (> 1 % of dry weight), with a small peak of magnetic susceptibility and where the geochemical analysis shows a minor component of goethite. The second layer at ~50 cm depth is ~15 cm thick made of mixed yellow sand with silty-clay pockets, broken shell fragments, poor sorting and with low peak magnetic susceptibility. It is rich in organic matter compared to the other layer, and the geochemical analysis shows minor amounts of halite.

Several samples were collected below and above the high energy sedimentary layers but, unfortunately, their content did not contain enough carbon for dating. The two shell (gastropod) samples collected at 75 cm and 77 cm depth (well below the lowermost high energy sedimentary layer, Fig.S2-2) have calibrated dates of 32971-34681 and 34362-36931 BC, respectively (Table 2b). These ages may well be due to mixed and/or reworked sedimentation.

Core 3: This core located 270 m from the shoreline near the outlet (lowland between high dunes) that allowed tsunami wave inundation (Fig. 2b and Fig. S2 – 3). It revealed three high energy sedimentary layers. The first layer is ~25 cm deep and corresponds to a 26 cm thick pale brown clay characterized by broken shells fragments and sediments rich in organic matter. The second layer at ~70 cm depth is 17.5 cm thick and characterized by white sand laminated at the top with a low peak of magnetic susceptibility, and with high organic matter > 2 % of dry weight. The third layer, 106 cm below the surface, is 32 cm thick and characterized by yellow sand with minor illite and broken shell fragments.

Two shell samples were collected for dating at 37 cm and 45 cm depth and have calibrated dates of 43618 BC and 34218-37224 BC respectively (Fig.S2-3 and Table 2b). These two samples are located within the stratigraphic high energy sedimentary layer 2 and may correspond to reworked sediments due to the high energy sedimentation during the catastrophic event.

Core 4: The core is located 435 m from the shoreline and shows sedimentary units where we identify two high energy sedimentary layers with low magnetic susceptibility (Fig. S2 - 4). The first layer (7 cm thick) is a white sand at ~12.5 cm depth with poorly sorted sediments, broken shell fragments with organic matter > 2 % of dry weight of total sediment fraction.

The second layer is pale yellow sand at ~102 to 130 cm depth, characterized by broken shell fragments with a minor amount of illite and gypsum.

One shell sample collected for dating at 37 cm depth provides a calibrated date of 32887-34447 BC (Table 2b). This sample, located in the stratigraphic high energy sedimentary layer 1, results from high energy reworked sedimentation during the catastrophic event (Fig. S2-4).

Core 5: The core is the southernmost in the El Alamein site, located 490 m from the shoreline (Fig. 2 b; Fig. S2 - 5). The core reaches a depth of 73 cm and the sedimentary succession does not show any catastrophic sedimentary layer of high energy sedimentary origin. According to its content, core 5 may show the limit of the inundation area with respect to at least the first and second high energy sedimentary layers.

Core 6: This core is located south of the sand dunes, 320 m from the shoreline (Fig. 2 b). It is characterized by three high energy sedimentary layers (Fig. S2 - 6). The first layer is a ~24 cm thick pale yellow sand with broken shells fragments (between 5 and 26 cm depth) and poorly sorted sediments rich in organic matter (larger than 2.5 % of dry weight). The second layer (~18.5 cm thick) at 50 - 75 cm depth is characterized by yellow sand with mixed gastropods and bivalves, and a high value of magnetic susceptibility at the base of the layer. The third layer at 130 cm depth is ~20 cm thick and rich in organic matter, characterized by white sand mixed with gravel and pebble and bioclasts.

Three samples were collected for dating in core 6. The first sample is a gastropod shell at ~45 cm depth and shows a calibrated age of 35002-37441 BC. The second and third samples are coral and charcoal fragments at ~60 cm and ~80 cm depth that gave calibrated ages of 42776-69225 BC and modern (younger than 1650AD). The first gastropod sample is above the high energy sedimentary layer 2 while the second coral sample was within the stratigraphic high energy sedimentary layer 2 (Fig S2-7). These samples may result from mixed sedimentation and reworking due to high current waves.

Core 7: This core was located 273 m from the shoreline (Fig. 2 b). It is characterized by sedimentary units that may include three high energy sedimentary layers within the 120 cm deep core (Fig. S2 - 7). The first layer (~14 cm depth) is a 6 cm thick brown sand with broken shell fragments and a considerable amount of cement gypsum with a minor amount of Illite and goethite. It is rich with organic matter (> 2 % of dry weight) of a swampy environment and the noticeable peak of magnetic susceptibility. The second layer at 50 cm depth is 20 cm thick and characterized by laminated pale brown clay mixed with gravel and pebbles at the bottom. The third layer at 115 cm depth is 15 cm thick and characterized by white sand, poorly sorted sediments with a minor amount of pyrite.

A single shell fragment sample was collected at 17 cm depth within high energy sedimentary layer 1 for radiocarbon dating and provides an age of 293-1113 BC.

Core 8: This core is located 214 m from the shoreline (Fig. 2 b). Three high energy sedimentary layers are recognized (Fig.S2 - 8). The first layer is a 16 cm thick pale yellow silty clay at ~14 cm depth, rich in organic matter, with a minor amount of goethite and bioclasts rich. The second layer (~52 cm depth) is a 22 cm thick pale yellow silty-clay with broken shells, characterized by a high peak of magnetic susceptibility and rich in organic matter (>2.5 % of dry weight). The third layer (~128 cm depth) is 9 cm thick and, characterized by pale yellow sand with broken shell fragments and poorly sorted angular gravel sized clasts. No samples were suitable for dating in this core.

Core 9: The core is located 130 m from the shoreline. Three high energy sedimentary layers are recognized (Fig. 5 b; Fig. S2 - 9). The first layer (~16 cm depth) is a 13 cm thick white sand with a high content of organic matter and rip up clasts that appear in X-ray scanning characterized by highly broken shell fragments. The second layer at 67 cm depth is 22 cm thick and characterized by white sand, with a peak of magnetic susceptibility, high content of organic matter larger than (5 % of dry weight). The third layer at 139 cm depth is 14 cm thick and characterized by broken shell fragments and white sand with highly angular sediments that reflect the poor granulometric sorting.

Two samples were collected for dating in core 9. The first sample is a gastropod shell located at 24 cm depth within the high energy sedimentary layer 1 and gives a calibrated age of 1052-1888 BC. The second sample at 55 cm depth is a bivalve (lamellibranch) located above the high energy sedimentary layer 2 dated at 40521-43169 BC calibrated age.

Core 10: The core is located 245 m from the shoreline (Fig. 2 b). Three high energy sedimentary layers are recognized (Fig. S2 - 10). The first layer (~19 cm depth) is a 9 cm thick brown silty clay with broken shell fragments, rich in organic matter (> 4 % of dry weight) and high peak of magnetic susceptibility; rip up clasts and laminations appear in X-ray scanning. The second layer (38 cm thick) is a brown sand at 48 cm depth with broken fragments of shells, peak of magnetic susceptibility and high organic matter (> 1.5 % of dry weight) at the bottom of the layer. The third layer is a 28 cm thick pale yellow sand at 101 cm depth. It is characterized by rich organic matter and poorly sorted sediments.

Two samples were collected for dating in core 10. The first sample, located in the high energy sedimentary layer 1, is a shell fragment at 24 cm depth that gives a calibrated age of 2623-3521 BC. The second sample, located in the high energy sedimentary layer 2, is a rodent bone at 70 cm below the surface with estimate calibrated age of 41256-46581 BC (see Table 2b).

Core 11: The core is located 151 m from the shoreline (Fig. 2 b). Three high energy sedimentary layers are recognized (Fig.S2 - 11). The first layer is 10 cm thick white sand with broken shell fragments at ~19 cm depth. The layer shows high magnetic susceptibility, rich organic matter (> 4 % of dry weight) with a high percent of gypsum (>50%). The second layer (76 cm depth) is a 9 cm thick white sand with broken shell fragments, a high peak of magnetic susceptibility and organic matter larger than 1.5 % of dry weight. The third layer is a 21 cm thick grey silty sand with broken shell fragments at 107 cm depth. It shows poor sorting, high organic rich matter and a minor amount of illite and gypsum.

Eight samples were collected for dating in core 11. The sedimentary units at 112 - 175 cm depth (core bottom) and related succession of ages between 3943 BC and 2475 BC (from shell gastropods and a charcoal fragment; see Table 2 b), may indicate a consistent dating of the high energy sedimentary layer 3. However, the first sample (gastropod shell) at ~20 cm depth gives an age of 3638-4328 BC, the second sample (broken shell) at 62 cm depth with an age at 17869 - 18741 BC, and the 33294 – 36120 BC and 2619 – 3386 BC out of sequence dating (Table 2 b).

Core 12: The core is located 127 m from the shoreline (Fig 2 b). Four high energy sedimentary layers are recognized in section 1 and one high energy sedimentary layer in section 2 (Fig. S2 – 12 a, b). The first layer is ~7.5-cm-thick at ~19-cm-depth and is made of poorly sorted white sandy deposits, and highly broken gastropods and lamellibranch fossils. The layer is characterized by high value of organic matter and low peak magnetic susceptibility. The second layer is ~13-cm-thick white sandy deposits intercalated with coarse brown sand at ~32.5-cm-depth. It is characterized by horizontal lamination, poorly sorted sediments, rich in organic matter and high peak of magnetic susceptibility. The third layer is ~25-cm-thick grey sandy clay at 89-cm-depth, with laminations at the bottom of the deposit, vertically aligned gastropods, broken shell fragments, rich in total organic matter and a low peak of magnetic susceptibility. A fourth high energy sedimentary layer of medium to fine pale yellow sand, with broken shell fragments, is identified in section 2 (Fig. S2 – 12 b) at 151 cm depth. It is characterized by poor sorting, low peak of magnetic susceptibility, a large amount of organic matter (> 5.5 % of dry weight) and high amount of gypsum.

Five samples were collected for dating in core 12. In core section 1, the first sample is a gastropod found at 44 cm depth that gives an age of 3367-3366 BC. The second sample is a shell found at 108 cm depth and shows an age of 3097-3950 BC (Table 2 b). The third sample is a gastropod found at 114 cm depth dated at 3331-4050 BC. The fourth and fifth samples in core section 2 are gastropod shells found at 117 cm and 135 cm depth with calibrated age of 39560- 40811 BC and 3365-4071 BC, respectively (Table 2 b). The fourth sample is off sequence with respect to the other samples and may result from sediment transport and reworking due to high energy waves. The other samples with ages from 4071 to 2457 BC are comparable to the sedimentary succession of core 11.

Results: The sedimentary deposits in the El Alamein lagoon also result from intercalated high-energy marine deposits into low energy marine and alluvial deposits with reworked sedimentation. A first observation in almost all cores is the existence of the white sand layer with broken shells of marine origin located ~10 cm to 170 cm depth in El Alamein site, and the identified three to four high energy sedimentary layers.

6. Summary of results from trenching and coring

The cores and trenches in both Kefr Saber and El Alamein sites expose three main layers characterized by fine and coarse sand mixed with bioclasts. We assume these indicate the occurrence of high energy and catastrophic sedimentary deposits in the coastal lagoon environment (Figs. 2 a, b, and c, and Fig. 3). Although the two studied sites are ~200 km apart, a white sandy layer with broken shells is found in all trenches (see Fig. 3 and supplemental material S1 a, b, c, d, e) and cores (except for core 5, see Figs. 5 a and b, and supplemental material in Fig. S2 – 1 to 12). The recurrent white sandy deposits in trenches and cores is visible as coarse sand units mixed with gravel and broken shells that become finer-grained and thinner landward (see trench P4, Fig. 3) or disappear when distant from the shore (core 5, Fig. S2 – 5). The high energy sedimentary characteristics within four layers in the ~ 2 m thick sedimentary units suggest that these layers are tsunami deposits rather than storm deposits.

In most cores (Figures. 5 a and b, and supplemental material Fig. S2 – (1 – 12)), the first tsunami layer is ~7.5-cm-thick at ~19 cm-depth and is made of poorly sorted white sandy deposits with broken gastropods and lamellibranch (shell) fossils. This layer is characterized by bi-modal grain size distribution with high value of organic matter and low peak of magnetic susceptibility with a rich content in carbonates and quartz. Goethite and pyrite heavy minerals were found in the cores at the base of layer 1, which also contains rip up clasts from underlying sediments. The second layer is ~13-cm-thick at ~32.5-cm-depth and characterized by white sandy deposits intercalated with laminated coarse brown sand, very poor sorting of sediments, rich in organic matter and with a low peak of magnetic susceptibility. Pebbles are found at the base of this layer which reflects a loadcast sedimentary structure. A considerable amount of heavy minerals, like goethite and pyrite can be found in this layer. The third layer is ~25-cm-thick at ~89-cm-depth and is made of grey sandy clay, with a high peak of magnetic susceptibility, laminations at the bottom of deposits, vertically aligned gastropods, broken shell fragments, and rich in total organic matter. In all three layers, the poorly sorted sediments and organic content are greater than 5 % of dry weight in the high energy deposits and tsunami records. These characteristics at the El Alamein site lead us to interpret the three sedimentary layers as tsunami deposits. The tsunami layers and their catastrophic content are identified in photography, X-rays, magnetic susceptibility, organic/mineral content and by the existence of mixed coarse and fine sand with broken marine shells. A main difficulty, however, is the age determination of the tsunami layers due to the mixed radiocarbon dates that range between old (50000 year BP - 13430 year BP) and young (5065 year BP - 125 year BP) ages in all cores.

In a synthesis of all dated units in trenches and cores in Figures 4 and 6, the sedimentary succession of low energy lagoon, marine and alluvial deposits intercalated with high-energy deposits provides evidence for the identification of four tsunami deposits at Kefr Saber and El Alamein sites. In the case of Kefr Saber trenches, the dating of charcoal fragments allows the bracketing of a tsunami event with a simulated age between AD 137 and AD 422, which includes the AD 365 western Crete earthquake (Figs. 4 and Table 2 a). The dating of sedimentary units at the El Alamein site turned out to be more complex due to highly reworked sedimentation and significant mix of old (> 13000 year BP) and young ages (< 5500 year BP; Table 2 b). Using the latter ages, the radiocarbon dating (including the Oxcal Bayesian analysis) of shells, bone and charcoal fragments at the El Alamein site (Fig. 6) results in a sequence of ages that allow the bracketing of an event W between 1434 BC and 1126 BC, and event X between AD 48 and AD 715, and event Y between AD 1168 and AD 1689, and an event Z between AD 1805 and AD 1935 (Figure 6). The three most recent simulated dates of tsunami events X, Y and Z might correlate with the seismogenic tsunamis of AD 365, AD 1303 and AD 1870 reported in catalogues (Table 1).

In the north of the trench sites at Kefr Saber, the dating of shells Dendropoma (worm snails) of common species Dendropoma petraeum and Vermetus triquetrus of a sample collected in a large boulder (Long: 26° 55.154 and Lat.: 31° 26.385) provide a radiocarbon calibrated date of 940-1446 AD. The dating of Dendropoma collected in a boulder often marks the catastrophic coastal environmental change with displaced large boulders from an intertidal to shoreline position due to a tsunami event. The Dendropoma sample age at Kefr Saber may correlate with the 8 August 1303 earthquake and tsunami event that dragged large boulders onto the shoreline in agreement with the results of Shah-Hosseini et al. (2016). However, we could not identify the 1303 event in the trenches dug in the nearby lagoon at Kefr Saber.

Discussions and Conclusions

The identification of high energy sedimentary layers considered as tsunami deposits within the stratigraphic layers and results of radiocarbon dating allow us to identify four tsunami events (Figs. 4 and 5). The historical seismicity catalogue of the Eastern Mediterranean reported two significant tsunamigenic seismic events of the Hellenic subduction zone that affected the Mediterranean coast of Egypt: 1) The 21 July 365 earthquake (Mw 8.3 – 8.5; Stiros and Drakos, 2006; Shaw et al., 2008): and 2) the 8 August 1303 earthquake (Mw 7.8 – 8.0; Abu Al Fida, 1907; Ambraseys, 2009). A third tsunami event is also reported during the 24 June 1870 earthquake (Mw 7 - 7.5), but despite some debates on its occurrence, the inundation of the Alexandria harbour leaves no alternative on the tsunami waves on the Egyptian coastline (see section 2).

In our study, the distinction of tsunami sedimentary records from storm deposits is based on: 1) the record of the small number (3 to 4) layers while storm deposits controlled by seasonal climatic catastrophic events should have been more frequent (Lionello et al., 2006; Morton et al., 2007); 2) the existence of white sand sheet layers with broken shells at two sites (Kefer Saber and El Alamein) located ~200 km apart, bearing comparable age, structure and texture. This is a probable large tsunami; 3) the existence of organic rich clasts in sand sheets of some cores which indicates a catastrophic event with sufficient energy to break and erode the coastal barrier made of the shoreline rocky headlands, organic sediments and coastal dunes before reaching the lagoons; 4) the bimodal distribution of the grain size of sandy sedimentary units that include a large proportion of broken shells comparable to that of tsunami deposits (Scheffers and Kelletat, 2003); 5) the correlation between the simulated ages of tsunami layers from the radiocarbon dating and the large historical tsunamigenic earthquakes of the eastern Mediterranean (Figs. 4 and 6); 6) the high energy fining inland sedimentary sequence observed in trenches and cores which is related to tsunami deposits rather than storm deposits; and 7) the consistent depth of tsunami layers in cores of the El Alamein site (Fig. 7).

The magnetic susceptibility measurements along the cores which normally have a low peak value (values near the zero value) reflect a tsunami layer because it contains more carbonates and quartz than the underlying sediments. This rule is not coincided in all the cores due to presence of 0.91 -14.9 % of goethite and 1.3 - 21.02 % of pyrite iron oxides minerals. The value of the peak increase slightly above the zero value and reach 20-100 X 10^{-6} of magnetic susceptibility and this increase happen usually on the bottom of the tsunami layer.

As the sedimentary units in the 1 m to 2.6 m deep cores result from young deposition processes with high-energy marine units intercalated into low energy marine and alluvial deposits, we consider the radiocarbon dating older than 13430 year BP as a result of reworking of older rocks. Considering that the succession of 2.6 m uppermost deposits and related stratigraphic chronology are comparable in all cores in the El Alamein lagoon, we select the radiocarbon dates younger than 5500 year BP as representative of the recent sedimentary units that include tsunami layers. Using the radiocarbon dating of samples and related selected young ages, the sedimentary sequence of catastrophic layers and their ages obtained from the Bayesian simulation (Oxcal 4.2; Bronk-Ramsey, 2009) allow a correlation with the AD 365, AD 1303 and AD 1870 tsunamigenic earthquakes of the east Mediterranean Sea (Fig. 6). Hence, the dating of the three high energy sedimentary layers deposited along the Egyptian coastline at Kefr Saber and El Alamein sites correlate with the historically recorded seismogenic tsunamis of the Hellenic subduction zone. In addition, a fourth tsunami layer can be identified between 1126 BC and 1434 BC.

The lagoon sedimentary environment is a natural site of mixed and reworked marine and continental deposits, with significant erosion during major tsunamis that may explain the mixed radiocarbon dates (Tables 2 a and b). The mixing of old (older than 7000 years BP) and relatively young ages (younger than 2000 years BP) points to reworking of former deposits and redeposit in a lagoon environment. The apparently incoherent dating may result from: 1) the different type of samples used in radiocarbon dating such as charcoal, shell, bone and root (see Tables 2 a and b), and uncertainties that also result from different species of mollusks, and/or the reservoir effect; and 2) the old events as a result of eroded or transported deposits of previous tsunami or storm waves, which is difficult to evaluate since we found that the stratigraphic record of these high-energy events is probably incomplete or underestimated (Tables 2 a and b where among 30 samples 12 dated samples are > 30 ka).

Indeed, by considering the mixed sedimentation of reworked deposits intercalated with new units, our selection of samples younger than 2000 year BP at Kefr Saber, and younger than 5500 year BP at El Alamein allowed us to distinguish between old and new isotopic dating and infer a consistent chronology of tsunami deposits. For instance at the El Alamein lagoon, the clear separation between old (50000 year BP to13430 year BP) and young (5065 year BP - 125 year BP) radiocarbon dating, with no intermediate dates of sedimentation, confirms the different origin and processes of deposition. The radiocarbon dating indicates that the white sand and coarse mixed layers represent deposits that may result from tsunami events in 365, 1303 and 1870 (see Table 1). The first two events correlate with large earthquakes with Mw≥8 with well documented tsunami waves in the historical sources. The existence of the 365 tsunami seems to be widely recorded through widespread massive turbidities of the eastern Mediterranean region (Stanley and Bernasconi 2006; Polonia et al., 2016). The four recognized catastrophic layers in trenches and cores have physical and chemical characteristics that correlate with high energy environmental conditions of tsunami deposits. The four low magnetic susceptibility peaks of the four deposits also correlate with the high content of organic carbon matter and carbonates.

The record of past tsunami deposits along the Egyptian Mediterranean coastline is favored by the low topography and platform geomorphology. The coastal environment with similar lagoons and dunes with large areas with relatively flat morphology allowed the deposits of catastrophic marine deposits intercalated within alluvial deposits. The lagoon shapes elongated along the shoreline at Kefr Saber and El Alamein sites explain the similarity between the sedimentary units and the tsunami deposits. The correlation between the core deposits at El Alamein and trench deposits at Kefr Saber are marked by the dating of tsunami deposits and the correspondence of them with the AD 365 earthquake. The succession of sudden high-energy deposits with low energy and slow sedimentation may include reworked units that imply a disorder in the chronological succession. Although the results of dated shells may be suspicious (due to the unclosed mineralogical system), their reliability is tested with the comparison of nearby radiocarbon dating.

The size of past tsunamis can be compared with the thickness of catastrophic sedimentary units in trenches at Kefr Saber and core units of the El Alamein site. It appears that the tsunami deposits of the AD 365 tsunamigenic earthquake are thicker at Kefr Saber site than at the El Alamein site. In contrast, the thickness of sedimentary layers of the AD 1303 and AD 1870 are thicker at the El Alamein site. These results on the identification of past tsunamis and their repetition along the coastlines in Egypt and North Africa are decisive for the tsunami wave propagation and hazard models in the East Mediterranean Sea (Salama, 2017).

Acknowledgments

We are grateful to Prof. Hatem Odah and NRIAG administration, and staff for their keen efforts and help during the development of this work. We address our special thanks to the Egyptian Armed Forces for issuing permissions and their support during field work. We thank the North African Group for Earthquake and Tsunami studies (NAGET), Assia Harbi, Adel Samy, Hany Hassen, Mohamed Maklad, Mohamed Sayed for field support and discussions. We are grateful to the "*Centre d'Etudes Alexandrine"* for the lending of the COBRA instrument for coring. An earlier version of this manuscript was improved thanks to the reviewers Raphael Paris, Pedro Costa and Cristino Jose Dabrio Gonzalez, and to Grant Wilson (emergency office management in Perth, Australia). This research programme is conducted with the funding support of the ASTARTE EC project (Assessment, Strategy And Risk Reduction for Tsunamis in Europe - FP7-ENV2013 6.4-3, Grant 603839), the French-Egyptian IMHOTEP project, and the Academy of Scientific Research and Technology of Egypt.

Supplementary data

Supplementary data associated with this manuscript are:

- Figures S1 a, b,c, d and e of five trench logs of Kefr Saber site (trench P4 as Fig. 3).
- Figure S2 – 1 (section 2) to 10 of core descriptions of El Alamein site (cores 1 and 9 as Figs a and b).

References

Abbas, M.S., El-Morsy, M.H., Shahba, M.A. and Moursy, F.I.,: Ecological studies in coastal sand dune rangelands in the North-West of Egypt, Meeting of the Sub-network on Mediterranean Forage Resources of the FAO-CIHEAM Inter-regional Cooperative Research and Development Network on Pastures and Fodder Crops, Spai: , 389–393, 2008.

Abu al-Fida Ismail Ibn Hamwi (born 1273 – died 1331). : The Concise History of Humanity or Chronicles (in Arabic *'Tarikhu 'al-Mukhtasar fi Akhbar al-Bashar'* in 1329). Al-Husayniyah Press, Cairo, 2 volumes , 1112 p., 1907.

Ambraseys, N.N., Melville, C.P. and Adam, R.D.: The seismicity of Egypt, Arabia and Red Sea: A Historical Review, Cambridge University Press, 181 p., 1994.

Ambraseys, N.N., Melville, C.P. and Adams, R.D.: The seismicity of Egypt, Arabia and the Red Sea: a historical review. Cambridge University Press, 181p., 2005

Ambraseys, N.: Earthquakes in the Mediterranean and Middle East: A Multidisciplinary Study of Seismicity up to 1900, Cambridge University Press, 947 p., 2009.

Atwater, B.: Evidence for great holocene earthquakes along the outer coast of Washington state, Science, 236, 942 – 944, 1987.

Bondevik, S., S.K. Stormo, and G. Skjerdal.: Green mosses date the Storegga tsunami to the chilliest decades of the 8.2 ka cold event. Quaternary Science Reviews 45, 1–6, 2012

Ben Menahem, A.: Earthquake catalogue for the Middle East (92 B.C. to 1980 A.D.) Bollettino di Geofisica Teorica ed Applicata, 2I, 245-310, 1979.

Ben Menahem, A.: Four thousand years of seismicity along the Dead Sea rift, Journal of Geophysical Research, 96, 195–216, 1991.

Bronk Ramsey, C.: Bayesian analysis of Radiocarbon, Radiocarbon, 51(1), 337–360, 2009.

Bronk Ramsey, C., & Lee S.: Recent and Planned Developments of the Program OxCal, Radiocarbon, 55(2-3), 720-730, 2013.

Coumbary, A. : Sur le tremblement de terre du 24 juin 1870, Nouvelles Météorologiques Paris, 3, 200-201, 1870.

Chagué-Goff, C., Schneider, J.-L., Goff, J.R., Dominey-Howes, D., Strotz, L.: Expanding the proxy toolkit to help identify past events — lessons from the 2004 Indian Ocean Tsunami and the 2009 South Pacific Tsunami, Earth-Science Reviews, 107, 107–122, 2011

Costa, P.J.M., Andrade, C. Freire, Freitas, M.C., Oliveira, M.A., Cascalho, J., Application of microtextural and heavy mineral analysis in the study of onshore tsunami deposits – examples from Portugal, Scotland and Indonesia, Comunicações Geológicas, III, 1439-1443, 2014.

CMT catalogue: Centroid Moment Tensor catalogue of Harvard, http://www.seismology.harvard.edusearch.html.

De Martini, P.M., Barbano, M.S., Pantosti, D., Smedile, A., Pirrotta, C., Del Carlo, P., and Pinzi, S.: Geological evidence for paleotsunamis along eastern Sicily (Italy): An overview: Natural Hazards and Earth System Sciences, 12 (8), 2569–2580, 2012.

Donato, S.V., E.G. Reinhardt, J.I.Boyce, R. Rothaus & T. Vosmer.: Identifying tsunami deposits using bivalve shell taphonomy, Geology, 36 (3), 199-202, 2008.

El-Sayed, A., Korrat, I., and Hussein, H. M.: Seismicity and seismic hazard in Alexandria (Egypt) and its surroundings, Pure and Applied Geophysics, 161, 1003–1019, 2004.

Folk RL, Ward WC. : Brazos River bar: a study in the significance of grain size parameters. Journal of Sedimentary Petrology 27: 3–26, 1957.

Font, E., C. Nascimento, Baptista M.A. & Silva P.F.: Identification of tsunami induced deposits using numerical modelling and rock magnetism techniques: A study case of the 1755 Lisbon tsunami in Algarve, Portugal, Physics of the Earth and Planets Interiors, 182, 187–198, 2010

Frihy , O.E., Deabes, E. a., and El Gindy, A. a.: Wave Climate and Nearshore Processes on the Mediterranean Coast of Egypt: Journal of Coastal Research, 261, 103–112 , 2010.

Fokaefs, A., and G. A. Papadopoulos.: Tsunami hazard in the Eastern Mediterranean: strong earthquakes and tsunamis in Cyprus and the Levantine Sea, Natural Hazards, 40 (3), 503–526, 2007.

Galanopoulos, A.G.: The seismic sea-wave of 9 Iouliou 1956, Praktika Academy Athens, 32, 90–101, 1957.

Goff J, Dudley WC, de Maintenon MJ, Cain G, Coney JP.: The largest local tsunami in 20th century Hawaii, Marine Geology 226, 65–79, 2006

Goff, J.R., Lane, E., Arnold, J.: The tsunami geomorphology of coastal dunes, Natural Hazards Earth System Sciences, 9 (3), 847–854, 2009.

Guidoboni, E., Comastri, A. and Traina G.: Catalogue of Ancient Earthquakes in the Mediterranean area up to the 10th century, INGV-SGA, Bologna, 504 p., 1994.

Guidoboni, E., and A. Comastri : Catalogue of earthquakes and tsunamis in the Mediterranean area from the 11th to the 15th century, INGV-SGA, Bologna, 1037 p., 2005.

Hassouba, A.B.H.: Quaternary Sediments from the Coastal Plain of Northwestern Egypt (from Alexandria to Elomayid), Carbonates and Evaporites, 10 (1), 8–44, 1995.

Hall AM, Hansom JD, Williams DM, Jarvis J.: Distribution, geomorphology and lithofacies of cliff- top storm deposits: examples from the high-energy coasts of Scotland and Ireland. Marine Geology, 232, 131–155, 2006.

Hamouda, A.Z.: Numerical computations of 1303 tsunamigenic propagation towards Alexandria, Egyptian coast, Journal African Earth Science, 44, 37-44, 2006.

Hamouda, A.Z.: A reanalysis of the AD 365 tsunami impact along the Egyptian Mediterranean coast, Acta Geophysica, 58 (4), 687–704, 2009.

Jusseret, S. and Sintubin, M., Minoan Earthquakes: Breaking the Myth through Interdisciplinarity, Studies in Archaeological Sciences, Leuven University Press, 440 pp., 2017.

Lario, J., Zazo, C., Goy, J.L., Silva, P.G., Bardaji, T., Cabero, A., Dabrio, C.J., Holocene palaeotsunami catalogue of SW Iberia. Quaternary International 242, 196–200, 2011.

Lionello, P., J. Bhend, A. Buzzi, P.M. Della-Marta, S.O. Krichak, A. JansÃ, P. Maheras, A. Sanna, I.F. Trigo, and R. Trigo, Chapter 6 in Cyclones in the Mediterranean region: Climatology and effects on the environment", Elsevier, 4, 325-372, 2006.

Maamoun, M., Megahed, A. and Allam, A.: Seismicity of Egypt, NRIAG Bulletin, IV (B), 109–160, 1984.

Maramai, A., Brizuela, B., Graziani, L. : The Euro- Mediterranean tsunami catalogue. Annals of Geophysics, 57 (4), 1-26, 2014.

Marriner, N., Kaniewski, D., Morhange, C., Flaux, C., Giaime, M., Vacchi, M., and Goff, J.: Tsunamis in the geological record, making waves with a cautionary tale from the Mediterranean, Science Advances, 1-12, 2017.

Malik, J.N., Banerjee, C., Khan, A., Johnson, F.C., Shishikura, M., Satake, K., and Singhvi, A.K.: Stratigraphic evidence for earthquakes and tsunamis on the west coast of South Andaman Island, India during the past 1000years, Tectonophysics, 661, 49–65, 2015.

Matsumoto, D., H. Naruse, S. Fujino, A.Surphawajruksakul, T., Jarupongsakul, N., Sakakura & M. Murayama: Truncated flame structures within a deposit of the Indian Ocean Tsunami: evidence of syn-sedimentary deformation, Sedimentology, 55, .1559-1570, 2008.

Matsumoto, D., Sawai, Y., Tanigawa, K., Fujuwara, O., Namegaya, Y., Shishikura, M., Kagohara, K., Kimura, H., Tsunami deposit associated with the 2011 Tohoku-oki tsunami in the Hasunuma site of the Kujukuri coastal plain, Japan, Island Arc, 25, 269-385, 2016.

Maouche, S., Morhange, C. and Meghraoui, M.: Large boulder accumulation on the Algerian coast evidence tsunami events in the western Mediterranean, Marine Geology, 262 (1), 96-104, 2009.

Meltzner, A.J., K. Sieh, H.-W. Chiang, C.-C. Shen, B.W. Suwargadi, D.H. Natawidjaja, B.E. Philibosian, R.W. Briggs, and J. Galetzka, Coral evidence for earthquake recurrence and an A.D. 1390-1455 cluster at the south end of the 2004 Aceh-Andaman rupture, *J. Geophys. Res.***115**, B10402, doi:10.1029/2010JB007499, (2010).

Minoura, K., Imamura, F., Kuran, U., Nakamura, T., Papadopoulos, G. A., Takahashi, T., Yalciner, A. C.: Discovery of Minoan tsunami deposits. *Geology* 28(1):59–62. 2000.

Morhange, C., Marriner, N., Pirazzoli, P.A.: Evidence of Late-Holocene tsunami events from Lebanon, Z. Geomorphology, 46, 81–95, 2006.

Morton, R, A., Gelfenbaum, G. and Jaffe, B. E., Physical criteria for distinguishing sandy tsunami and storm deposits using modern examples, Sedimentary Geology, 200, 3, 184-207, 2007.

Nanayama, F., Satake, K., Furukawa, R., Shimokawa, K., Atwater, B.F., Shigeno, K., and Yamaki, S.: Unusually large earthquakes inferred from tsunami deposits along the Kuril trench, Nature, 424 (6949), 660–663, 2003.

Paris, R., F., Lavigne, P.,Wassmer, and J.,Sartohadi : Coastal sedimentation associated with the December 26, 2004 tsunami in Lhok Nga, West Banda Aceh (Sumatra, Indonesia). Marine Geology, 238, 93–106, 2007.

Papadopoulos, G.A., E. Daskalaki, A. Fokaefs and N. Giraleas.: Tsunami hazard in the Eastern Mediterranean Sea: strong earthquakes and tsunamis in the West Hellenic Arc and Trench System, Journal Earthquake and Tsunami, 4 (3), 145-179, 2010.

Papadopoulos, G.A., Minoura, K., Imamura, F., Kuran, U., Yalçiner, A., Fokaefs, A., Takahashi, T., Strong earthquakes and tsunamis in the East Hellenic arc. Research in Geophysics 2 (e12), 90–99. http://dx.doi.org/10.4081/rg.2012.e12. 2012.

Papadopoulos, G. A., Gràcia, E., Urgeles, R., Sallares, V., De Martini, P. M., Pantosti, D., González, M., Yalciner, A. C., Mascle, J., Sakellariou, D., et al.: Historical and pre-historical tsunamis in the Mediterranean and its connected seas: Geological signatures, generation mechanisms and coastal impacts, Marine Geology, 354, 81–109, 2014.

Polonia, A., Vaiani, S.C., de Lange, G.J.: Did the A.D. 365 Crete earthquake/tsunami trigger synchronous giant turbidity currents in the Mediterranean Sea?, Geology, 44, 191-194, 2016.

Poirier, J. P. and Taher, M.A.: Historical Seismicity in the near and Middle East, North Africa, and Spain from Arabic Documents (VIIth- XVIIIth Century). Bulletin Society Seismology American, 70 (6), 2185–2201, 1980.

Reimer PJ, Bard E, Bayliss A, Beck JW, Blackwell PG, Bronk Ramsey C, Buck CE, Edwards RL, Friedrich M, Grootes PM, Guilderson TP, Haflidason H, Hajdas I, Hatté C, Heaton TJ, Hogg AG, Hughen KA, Kaiser KF, Kromer B, Manning SW, Reimer RW, Richards

DA, Scott EM, Southon JR, Turney CSM, van der Plicht J.: Selection an treatment of data for radiocarbon calibration: an update to the International Calibration (IntCal) criteria, Radiocarbon, 55 (4), 1869-1887, 2013.

Salama, A.: Active tectonics and Paleo-tsunami records of the Northern Coast of Egypt, Ph.D thesis dissertation, University of Strasbourg, 429 pp., 2017.

Sayed, A.: Evaluation of the land resources for agriculture development. Case study: EL Hammam canal and its extension, NW coast of Egypt, PhD thesis dissertation, University of Hamburg, 241pp., 2013.

Salamon, A., Rockwell, T., Ward, S. N., Guidoboni, E. & Comastri, A.: Tsunami hazard evaluation of the Eastern Mediterranean: Historical analysis and selected modeling, Bulletin of the Seismological Society America, 97, 705–724, 2007.

Sawai, Y. Episodic emergence in the past 3000 years at the Akkeshi estuary, Hokkaido, northern Japan. *Quat. Res.* **56,** 231-241 (2001).

Schmidt, J.F.: Studien ueber Erdbeben. 1-136, 316-360, Leipzig, 1879.

Scheffers, A. & Kelletat, D. (2003): Sedimentologic and Geomorphologic Tsunami Imprints Worldwide – a Review. Earth Science Reviews, 63, 1-2, 83-92.

Shah-Hosseini, M., Saleem, A., Mahmoud, A. and Morhange, C.: Coastal boulder deposits attesting to large wave impacts on the Mediterranean coast of Egypt, Natural Hazards, 83 (2), 849-865, 2016.

Shaw, B., Ambraseys, N. N., England, P.C., Floyd, M., Gorman, G.J., Higham, T.F.G., Jackson, J., Nocquet, J-M., Pain, C. C., and Piggott, M. D.: Eastern Mediterranean tectonics and tsunami hazard inferred from the AD 365 earthquake, Nature Geoscience, 1 (April), 268–276, 2008.

Soloviev, S.L., Solovieva, O.N., Go, C.N., Kim, K.S., and Shchetnikov, N.A.: Tsunamis in the Mediterranean Sea 2000 B.C.-2000 A.D., Advances in Natural and. Technological Hazards Research, Kluwer Academic Publishers, Dordrecht,. Netherlands, 13, 237 p., 2000.

Stanley, J.D. – Bernasconi, M.P.: Holocene depositional patterns and evolution in Alexandria's eastern harbor, Egypt, Journal of Coastal Research, 22 (2), 283-297, 2006.

Stiros, S. C.: The AD 365 Crete Earthquake and Possible Seismic Clustering During the Fourth to Sixth Centuries AD in the Eastern Mediterranean: A Review of Historical and Archaeological Data, Journal of Structural Geology, 23, 545–562, 2001.

Stiros, S., and Drakos, A.: A fault model for the tsunami-associated magnitude >8.5 Eastern Mediterranean, AD 365 earthquake, Zeitschriftfür Geomorphologie, 146, 125–137, 2006.

Spiske M, Bo ̈cz Z, Bahlburg H.: The role of porosity in discriminating between tsunami and hurricane emplacement of boulders—a case study from the Lesser Antilles, southern Caribbean, Earth Planet Science Letters, 268, 384–396, 2008.

Switzer, A. D. and Jones, B.G.: Large scale washover sedimentation in a freshwater lagoon from the southeast Australian coast: sea level change, tsunami or exceptionally large storm?, The Holocene, 18 (5), 787-803, 2008.

Szczucinski, W., N. Chaimanee, P. Niedzielski, G. Rachlewicz, D. Saisuttichai, T. Tepsuwan, S.Lorene& J. Siepak : Environmental and geological impacts of the 26 December 2004 Tsunami in coastal zone of Thailand- Overveiw of short and long term effects. In: Polish Journal of Environmental studies, 15 (5), 793-810, 2006.

Taymaz, T., Westaway, R., and Reilinger, R.: Active faulting and crustal deformation in the Eastern Mediterranean region, Tectonophysics, 391, 1–9, 2004.

Tinti, S., Maramai, A. and Graziani, L. (2001a). "A New Version of the European Tsunami Catalogue: Updating and Revision", Natural Hazards and Earth System Sciences, 1, 255-262, 2001.

Tinti, S., Manucci, A., Pagnoni, G., Armigliato, A., and Zaniboni, F.: The 30 December 2002 landslide-induced tsunamis in Stromboli: sequence of the events reconstructed from the eyewitness accounts, Natural Hazards and Earth System Science, 5 (6), 763–775, 2005.

Tyuleneva, N., Braun, Y., Katz, T., Suchkov, I., Tchernov, B.N.G.: A new chalcolithic-era tsunami event identified in the offshore sedimentary record of Jisr al-Zarka (Israel) , Marine Geology (article in press), 1-12, 2017.

Tuttle, M.P., Ruffman, A., Anderson, T., and Jeter, H.: Distinguishing tsunami from storm deposits in eastern North America: the 1929 Grand Banks tsunami versus the 1991 Halloween storm, Seismological Research letters, 75, 117-31, 2004.

Yalciner, A., Zaytsev, A., Aytore, B., Insel, I., Heidarzadeh, M., Kian, R., and Imamura, F.: A Possible Submarine Landslide and Associated Tsunami at the Northwest Nile Delta, Mediterranean Sea: Oceanography, 27, (2), 68–75, 2014.

Figure captions

Figure1: Seismicity (instrumental with M> 5.5) and main tectonic framework of the east Mediterranean regions. Black boxes indicate the paleoseismic sites of Kefr Saber and El Alamein east of the Nile delta. The major historical earthquakes (blue box) of AD 365 (Mw 8 – 8.5), AD 1303 (Mw ~8) and AD 1870 (Mw > 7 – 7.5) are located along the Hellenic subduction zone according to Guidoboni et al. (1994), Stiros (2001); Ambraseys (2009); Papadopoilos et al. (2014) and Jusseret and Sintubin (2017). Focal mechanisms are CMT-Harvard.

Figure 2: Location of trenches and core sites at (a) Kafr Saber, (b) El Alamein (see Figure 1), and (c) Dune ridge and a lagoon south of the Mediterranean Sea as a selected site for coring and trenching at EL Alamein site.

Figure 3: a) Trench (P4) panorama at Kefr Saber, and (b) description of sedimentary layers of trench P4 with carbon dating sampling (yellow flags). The horizontal ruler indicates 20 cm scale.

Figure 4: Radiocarbon dating calibrated with probability density function (pdf) using Oxcal version 4.2 (Bronk-Ramsey, 2009) and chronology of sedimentary layers and tsunami record of trenches at Kefr Saber. The dating characteristics are in Table 2 a. The Bayesian dating simulation of the white sandy unit in Fig. 3 b can be correlated with the 365 AD tsunami event.

Figure 5: a) Core 1 log description with X-ray scanning, lithology log, magnetic susceptibility, mean grain size, sediment sorting, total organic and inorganic matter and bulk mineralogy. The arrows show the high values of each measurement that may correlate with tsunami deposits.

b) Core 9 log description with X-ray scanning, lithology log, magnetic susceptibility, mean grain size, sediment sorting, total organic and inorganic matter and bulk mineralogy. The arrows show the high values of each measurement that may correlate with tsunami deposits.

(Similar illustrations of cores 2 to 12 are in supplemental materials).

Figure 6: Radiocarbon dating calibrated with probability density function (pdf) using Oxcal version 4.2 (Bronk-Ramsey, 2009) and chronology of sedimentary layers with dated tsunami records at El Alamein. The dating characteristics are in Table 2 b. Black pdfs refer to the dated samples and red pdfs are simulated dating of the four tsunami records. Three sedimentary records are correlated with the historical earthquake and tsunami catalogue of the eastern Mediterranean (see Table 1).

Figure 7: Depth distribution of tsunami layers in cores at the El Alamein site (see core locations in Fig. 2 b). The depth correlation of paleotsunami layers indicates the consistent succession of deposits in the lagoon. Deposits of layers 1, 2 and 3 are related with tsunami events 1870 AD, 1303 AD and 365 AD of the East Mediterranean Sea (see Fig. 6 and Table 1). Layer 4 corresponds to tsunami event 1491 – 1951 BC and is not reported in tsunami catalogues.

TABLES

Table 1: Major earthquakes of the eastern Mediterranean with tsunami wave records in northern Egypt. Estimated magnitudes are given in Mw when calculated and in M when estimated.

Table 2 a: Radiocarbon dating samples and calibrated age at Kefr Saber site using OxCal v4.2.4 (Bronk-Ramsey, 2013). White background color is for charcoal and grey for shell ages.

- CIRAM Lab. science for art cultural heritage ,archeology department http://www.ciram-art.com/en/archaeology.html
- Poznan Lab. Poznan Radiocarbon Laboratory, Poland, email: c.fourteen@radiocarbon.pl http://radiocarbon.pl/index.php?lang=en.
- Beta Analytic radiocarbon dating, Miami, Florida, USA http://www.radiocarbon.com/, e-mail: lab@radiocarbon.com

Table 2 b: Radiocarbon dating samples and calibrated date in El Alamein site using OxCal v4.2.4 (Bronk-Ramsey, 2013). Underlined dark grey color is for bone, grey for shell, light grey for root and white for charcoal samples.

- CIRAM Lab. science for art cultural heritage ,archeology department http://www.ciram-art.com/en/archaeology.html
- Poznan Lab. Poznan Radiocarbon Laboratory, Poland, email: c.fourteen@radiocarbon.pl http://radiocarbon.pl/index.php?lang=en.
- Beta Analytic radiocarbon dating, Miami, Florida, USA http://www.radiocarbon.com/, e-mail: lab@radiocarbon.com

TABLES

Table 1: Major earthquakes of the eastern Mediterranean with tsunami wave records in northern Egypt. Estimated magnitudes are given in Mw when calculated and in M when estimated.

Date	Epicentre	Estimated Magnitude	Comment	Reference
21 July 365	Western Crete	8.3 – 8.5 (M_w)	Tsunami northern Egypt	Stiros and Drakos, 2006; Shaw et al., 2008, Hamouda 2009
18 Jan. 746	Dead Sea Fault	7.5 (M)	Tsunami eastern Medit.	Ambraseys, 1962
881 - 882	Palestine	?	Tsunami in Alexandria & Palestine	Galanopoulos A., 1957
4 Jan. 1033	Jordan Valley Fault	7.4 (M)	Tsunami northern Egypt	Ambraseys, 1962
18 Jan. 1068	Northern Lebanon	6.9 (M)	Waves in Lebanon Until northern Egypt	Ambraseys, 1962, Soloviev et al., 2000
8 Aug. 1303	Karpathos & Rhodos islands	8 (M)	>8-m-high wave in Alexandria	Abu al-Fida1329, Ambraseys 2009, Hamouda 2006
24 June 1870	Hellenic Arc	M_L 7.2	Inundation in Alexandria harbour	Ben-Menahem, 1979, Soloviev et al., 2000

Table 2 a: Radiocarbon dating samples and calibrate age at KefrSaber site using OxCal v4.2.4 (Bronk-Ramsey, 2013).

No.	Sample name	Laboratory Name	Type of samples	Depth (m)	Date BP	Calibrated. date
1	TSU P4 S2	CIRAM	Charcoal	61	Modern	-
2	TSU P4 S3	CIRAM	Charcoal	40	Modern	-
3	TSU P4 S4	CIRAM	Charcoal	15	Modern	-
4	TSU P1 S07B	Poznan	Charcoal	35	110.14±0.3	Modern
5	TSU P4 S6	Poznan	Charcoal	25	101.42 ± 0.68	1700 – 1920 AD
6	TSU P3 S2	Poznan	Charcoal	72	1075 ± 30 BP	890 – 1020 AD
7	KSB2S2	Poznan	Dendropoma	Boulder	890 ± 30 BP	940 - 1446 AD
8	TSU P5S3	Poznan	Charcoal	17	2060 ± 35 BP	180 – 30 AD
9	TSU P3S2	CIRAM	Charcoal	73	2000 BP	50-70 AD
10	TSU P5S1	Poznan	Charcoal	12	2145 ± 30 BP	360 – 50BC
11	TSU P5S4	Poznan	Charcoal	33	2590 ± 140	1050 – 350 BC

					BP	
12	TSU P5S2	Poznan	Charcoal	37	4560 ± 300 BP	4000 – 2400 BC
13	TSU P3S3	CIRAM	Charcoal	100	6240 BP	5300 – 5070 BC
14	TSU P4 S5	Poznan	Charcoal	60	15490 ± 70 BP	17200 – 15900 BC
15	TSU P1 S09B	CIRAM	Charcoal	53	40560 BP	39000-38250 BC

- CIRAM Lab. science for art cultural heritage ,archeology department http://www.ciram-art.com/en/archaeology.html
- Poznan Lab. Poznan Radiocarbon Laboratory, Poland, email: c.fourteen@radiocarbon.pl http://radiocarbon.pl/index.php?lang=en.
- Beta Analytic radiocarbon dating, Miami, Florida, USA http://www.radiocarbon.com/, e-mail: lab@radiocarbon.com

Table 2 b: Radiocarbon dating samples and calibrated date in El Alamein site using OxCal v4.2.4 (Bronk-Ramsey, 2013)

No.	Sample name	Laboratory Name	Type of samples	Depth (m)	Date BP	Calibrated date (2σ)
a	AL1 S1 (test pit)	CIRAM	charcoal	25	130±20	1680-1908 AD
b	AL1 S2 (test pit)	CIRAM	charcoal	56	190±20	1661-1931 AD
1	core 6/2 sa1	Poznan	charcoal	80	125±30	<1620 AD
2	core 1/1sa2	Poznan	Bone	50	1540±60	403-634 AD
3	core 7/1sa1	Poznan	shell	17	3000±30	293-1113 BC
4	core 9/1sa1	Poznan	gastropod	24	3320±30	1052-1888 BC
5	core10/1sa3	Poznan	shells	20	4515 ±30	2623-3521 BC
6	core11/2sa1	Beta analytic	roots	139	4810±30	2666 - 2817 BC
7	core11/2Sa4	Poznan	gastropod +shell	116	4500±35	2619-3386 BC
9	core11/2sa6	Poznan	gastropod	126	4405±35	2477-3368 BC
10	core 11 2_5	Poznan	gastropod	121	4360±40	2457-3366 BC
11	core 12/2sa1	Beta analytic	gastropod	108	4885±35	3097-3950 BC
12	core 12/2sa2	Poznan	gastropod	114	5000±35	3331-4050 BC
12	core 12/1 sa1	Poznan	gastropod	44	5065±30	3367-4072 BC
13	core 12/2sa4	Beta analytic	roots	135	5060±30	3365-4071 BC
14	core 11/1sa1	Beta analytic	gastropod	20	5230±30	3638-4328 BC
15	core 11-2	Beta analytic	charcoal	180	5020±30	3710-3943 BC
16	core 1/1sa1	Poznan	charcoal	40	13430±60	13985-14415 BC
17	core 11/2sa2	Beta analytic	shell	62	16900±60	17869-18741 BC

18	core2/1sa6	Poznan	gastropods	75	32000±360	32971-34681 BC
19	core 4/1sa1	Poznan	shell	28	31840±350	32887-34447BC
20	core11/2 sa11	Beta analytic	shells	152	32500±500	33294-36120 BC
21	core2/1sa4	Poznan	gastropods	77	35500±500	34362-36931 BC
22	core 3/1sa1	Poznan	shell	45	33500±600	34218- 37224 BC
23	core 6/1 sa6	Poznan	gastropod	45	34000±400	35002-37441 BC
24	core 12/2 sa3	Beta analytic	broken shell	117	37940±420	39560 -40811 BC
25	core 9/1sa5	Poznan	bivalve	55	40000±800	40521-43169 BC
26	core 10/1sa2	Poznan	bone	70	42000±1300	41256-46581 BC
27	core 3/1sa2	Poznan	bivalve	37	45000±2000	43618 BC
28	core 6/1sa9	Poznan	coral	60	50000±4000	42776-69225 BC

- CIRAM Lab. science for art cultural heritage ,archeology department http://www.ciram-art.com/en/archaeology.html
- Poznan Lab. Poznan Radiocarbon Laboratory, Poland, email: c.fourteen@radiocarbon.pl http://radiocarbon.pl/index.php?lang=en.
- Beta Analytic radiocarbon dating, Miami, Florida, USA http://www.radiocarbon.com/, e-mail: lab@radiocarbon.com

Figure 1

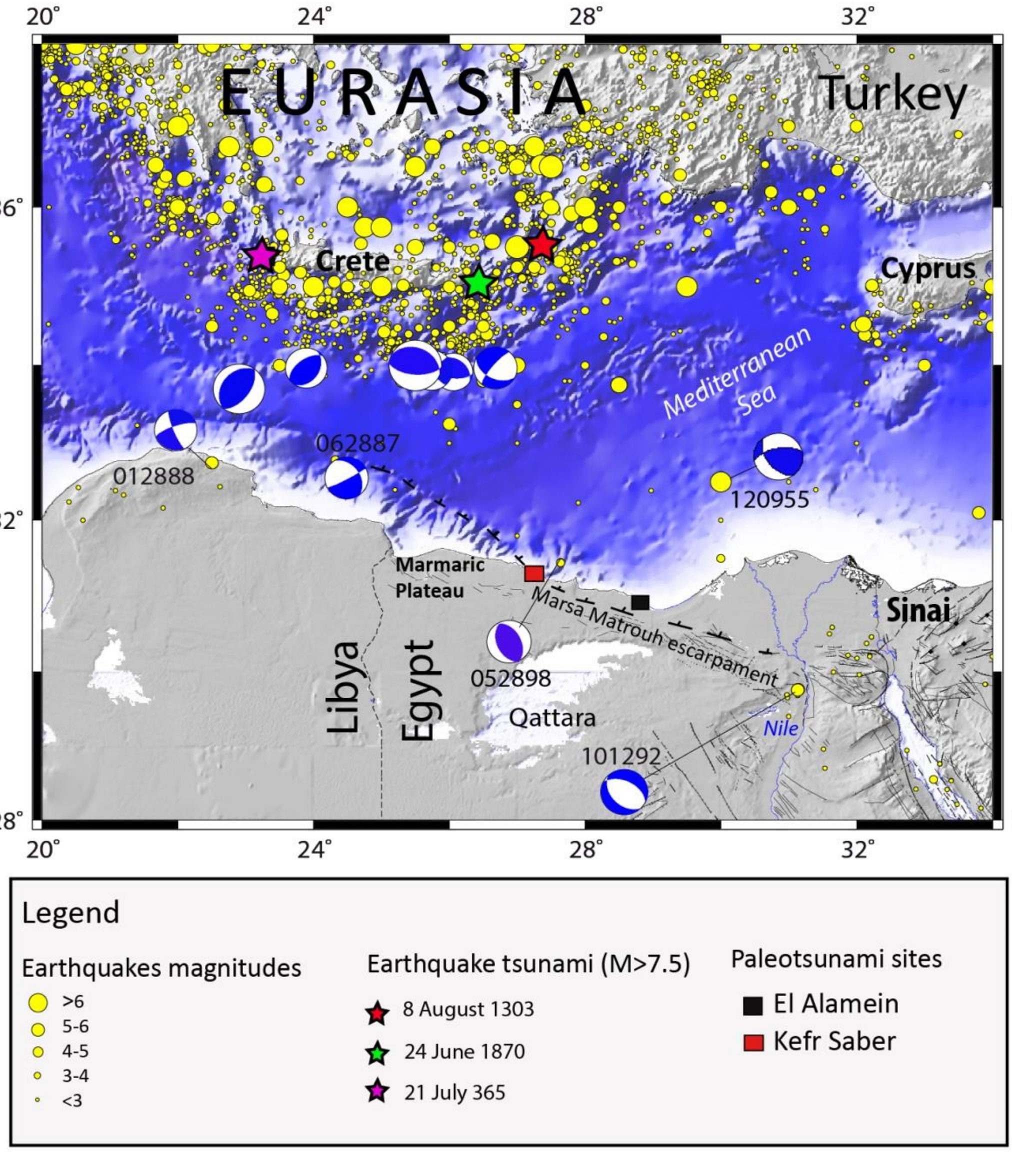
20°
24°
28°
32°
36°
32°
28°
EURASIA
Turkey
Crete
Cyprus
Mediterranean Sea
012888
062887
120955
Marmaric Plateau
Marsa Matrouh escarpment
Sinai
052898
Libya
Egypt
Qattara
Nile
101292
Legend
Earthquakes magnitudes
>6
5-6
4-5
3-4
<3
Earthquake tsunami (M>7.5)
8 August 1303
24 June 1870
21 July 365
Paleotsunami sites
El Alamein
Kefr Saber

Figure 2

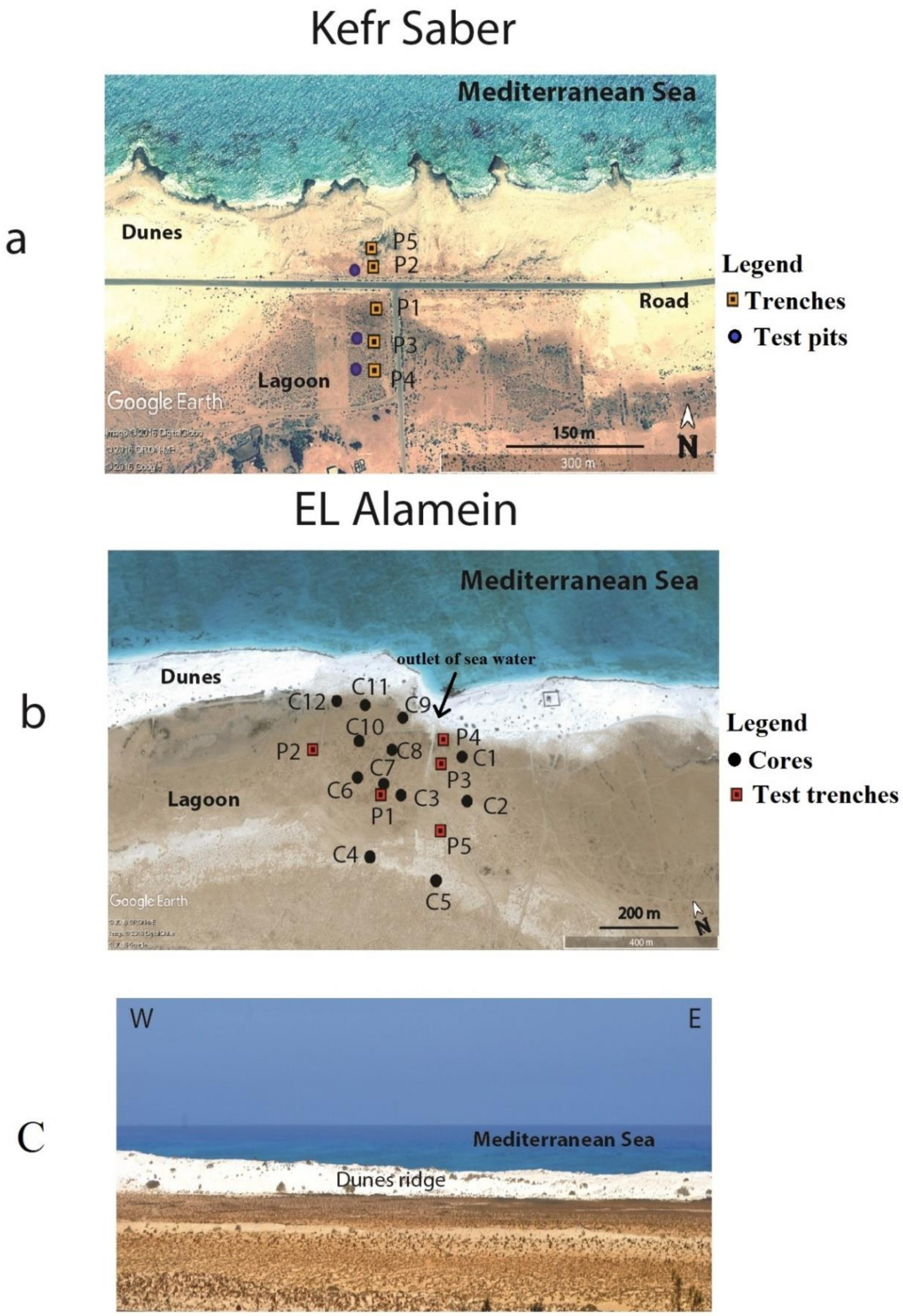
Kefr Saber
a
Mediterranean Sea
Dunes
P5
P2
P1
P3
P4
Road
Lagoon
Google Earth
150 m
300 m
N
Legend
Trenches
Test pits
EL Alamein
b
Mediterranean Sea
outlet of sea water
Dunes
C11
C12
C9
C10
P4
P2
C8
C1
C7
P3
C6
C3
C2
Lagoon
P1
P5
C4
C5
Google Earth
200 m
400 m
N
Legend
Cores
Test trenches
C
W
E
Mediterranean Sea
Dunes ridge

Figure 3

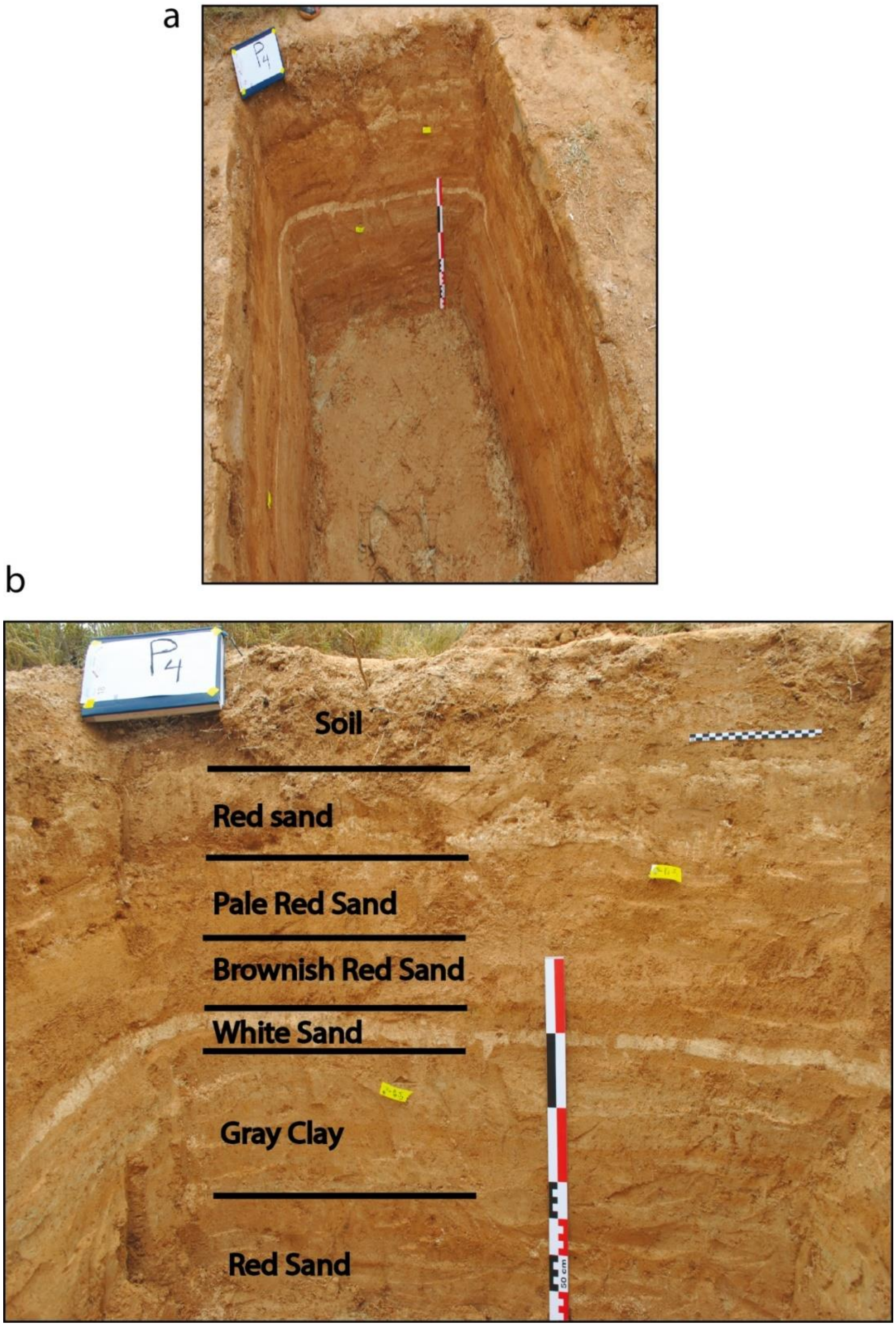
a
b
P4
Soil
Red sand
Pale Red Sand
Brownish Red Sand
White Sand
Gray Clay
Red Sand

Figure 4

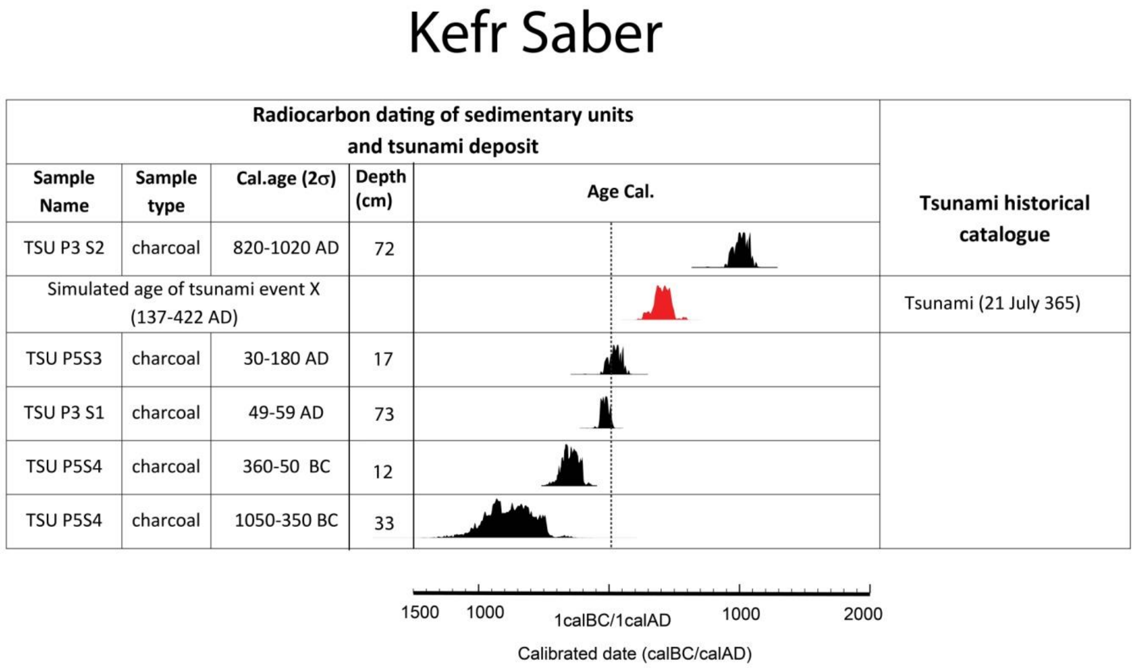

Kefr Saber

Radiocarbon dating of sedimentary units and tsunami deposit					Tsunami historical catalogue
Sample Name	Sample type	Cal.age (2σ)	Depth (cm)	Age Cal.	
TSU P3 S2	charcoal	820-1020 AD	72		
Simulated age of tsunami event X (137-422 AD)					Tsunami (21 July 365)
TSU P5S3	charcoal	30-180 AD	17		
TSU P3 S1	charcoal	49-59 AD	73		
TSU P5S4	charcoal	360-50 BC	12		
TSU P5S4	charcoal	1050-350 BC	33		

Figure 5 a

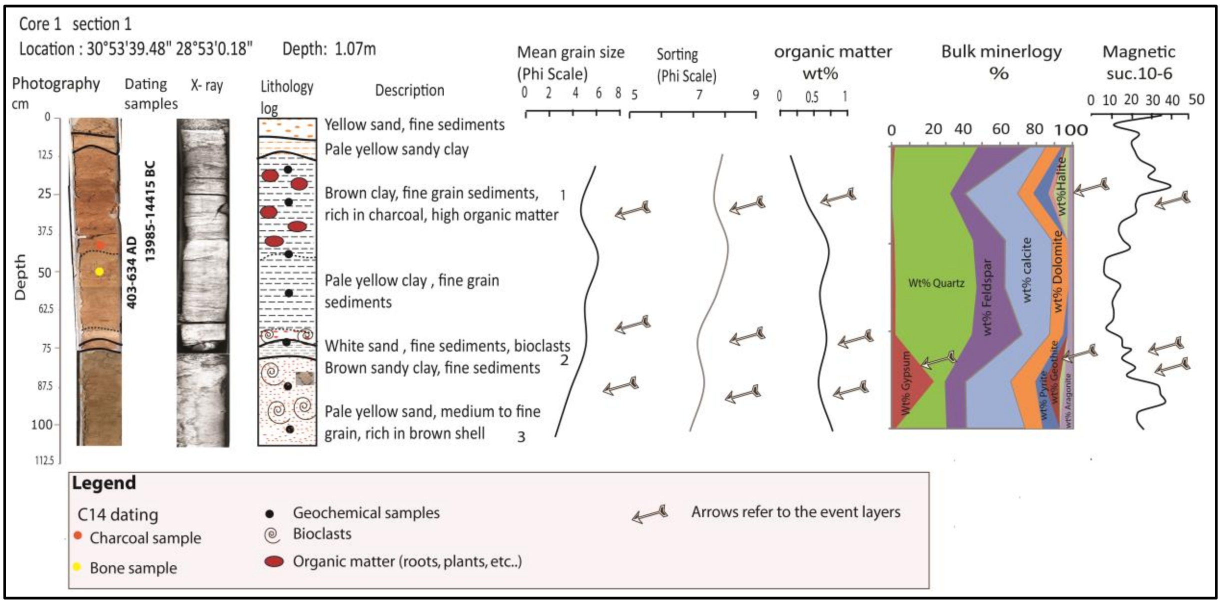

Figure 5b

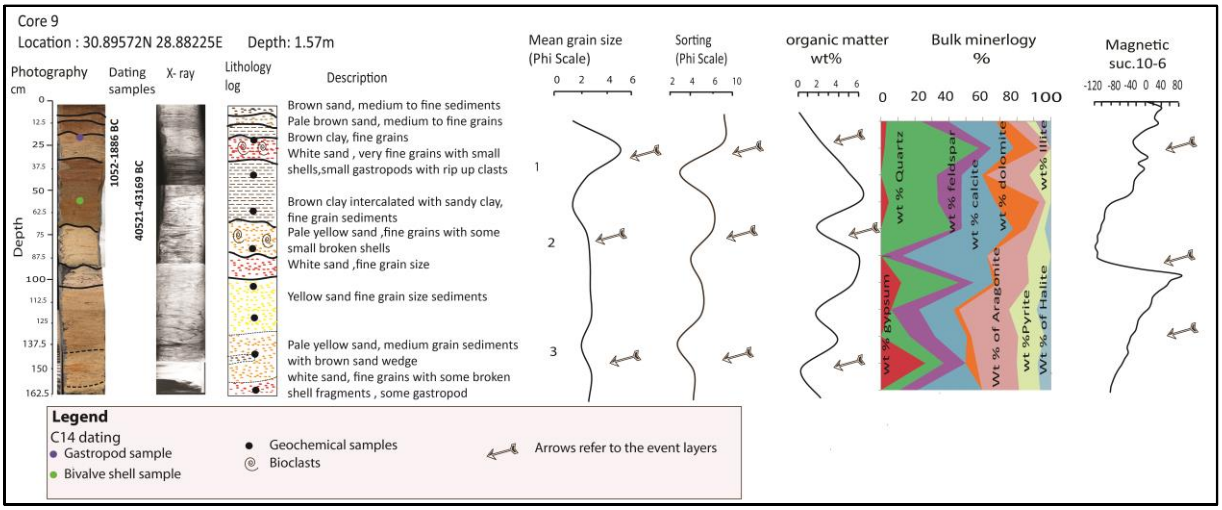

Figure 6

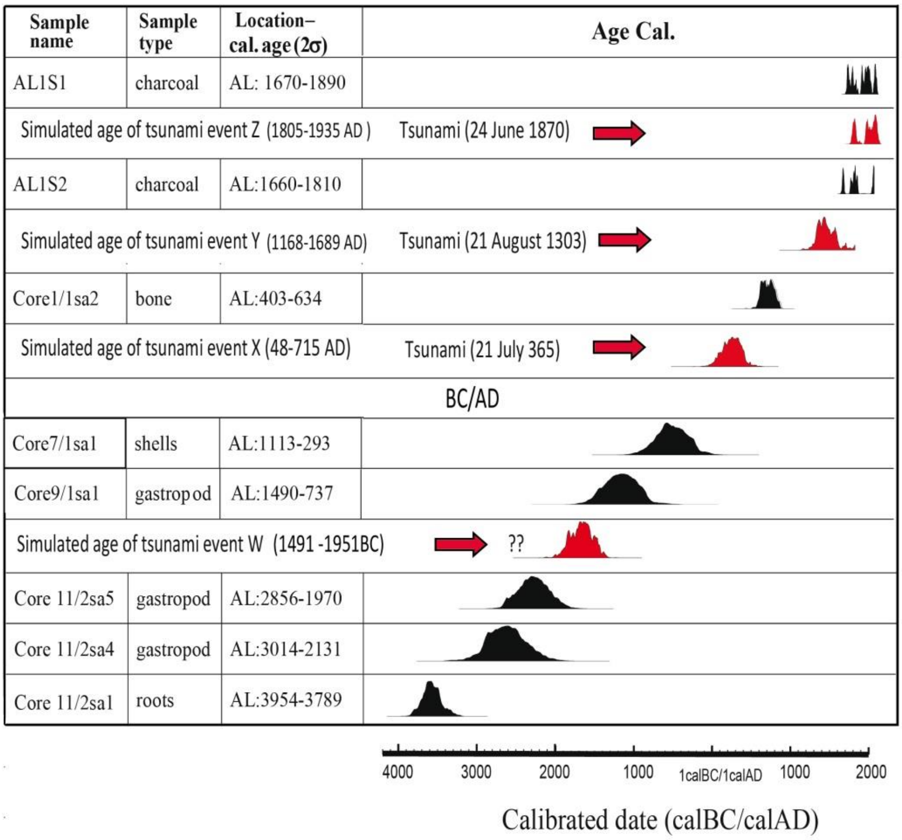

1018 Figure 7

1019

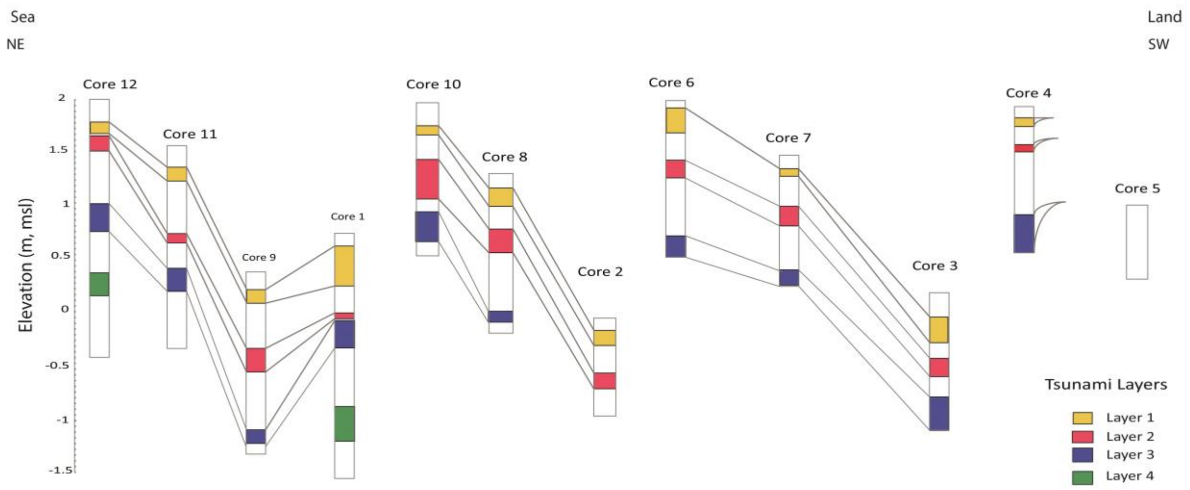

1020